

# Bonding of Tungsten and Graphite Using Spark Plasma Sintering for Divertor Component in LHD

Takanori MURASE<sup>1)</sup>, Tomohiro MORISAKI<sup>1,2)</sup>, Toshiaki SOGABE<sup>3)</sup> and Tomohiro SHIOZAKI<sup>3)</sup>

<sup>1)</sup>National Institute for Fusion Science, 322-6 Oroshi-cho, Toki, Gifu 509-5292, Japan

<sup>2)</sup>The Graduate University for Advanced Studies, SOKENDAI, Toki, Gifu 509-5292, Japan

<sup>3)</sup>ANAORI Carbon Co., Ltd., 6-20 Hatakeda-cho, Ibaraki, Osaka 567-0028, Japan

(Received 30 September 2022 / Accepted 28 November 2022)

The manufacturing of tungsten (W) - graphite bonded divertor components for the Large Helical Device (LHD) has been investigated. The spark plasma sintering method was used to bond W and graphite with titanium (Ti) interlayer. Small specimens were fabricated to investigate the bonding strength and to diagnose the bonding interface. The granular structure was formed in the grooved area on the graphite surface. It was suggested that this granular structure had affected the bonding strength.

© 2023 The Japan Society of Plasma Science and Nuclear Fusion Research

Keywords: tungsten, graphite, speak plasma sintering, LHD, divertor component

DOI: 10.1585/pfr.18.1205003

Graphite has been used as a plasma-facing material, e.g., divertor tiles in fusion experimental devices, because of its outstanding features such as high thermal conductivity, high-temperature strength, and low activation properties [1]. On the other hand, graphite has issues, i.e., high sputtering yield and tritium inventories. Thus, tungsten (W) is a strong candidate for plasma facing materials due to its low hydrogen isotope absorption, low sputtering yield, high recrystallization temperature, and high thermal conductivity. However, W has some disadvantages, such as a significant device mass due to its large density, or poor workability due to its high hardness, or difficulty bonding with other materials. To solve these issues of W and graphite, a method of coating graphite with W has been proposed [2–4]. In the Large Helical Device (LHD), W-coated graphite divertor tiles with vacuum plasma spray were installed to reduce carbon sputtering [5]. However, the thickness of the W layer was limited to a few hundred micrometers at most due to delamination limitations caused by strain energy accumulation, therefore microcracking occurred in W layer, since W layer was thin and its relative density was low.

If a W plate could be bonded directly to a graphite tile, dense W-bulk layer of millimeter-order thickness would be able to form, and the lifetime of the plasma facing material could be expected to be sufficiently long.

Direct bonding of W to C at high temperature and pressure settings, on the other hand, leads in the development of tungsten carbide at the bonding contact, reducing bonding strength [2]. Furthermore, recrystallization of W produced by high temperature processing is a major problem. When used as a structural material, W materials that

are not easily recrystallized must be used.

For attaching titanium (Ti) -zirconium (Zr) -molybdenum alloy to graphite, brazing [6], diffusion bonding [7], and spark plasma sintering (SPS) [8] have recently been proposed. For brazing and intermediate materials, Ti alloys and Zr alloys were used. In light of this research, we created a W bonded graphite divertor component for the LHD. Figure 1 shows an external view of the W bonded graphite divertor component for the LHD. The divertor component consists of a W plate of 1 mm thick and isotropic graphite IG-430U (Toyo Tanso Co., Ltd.). The diverter component of “two-part-type” is fixed to the cooling pipe by mechanical fastening with bolts. W and graphite were bonded with the SPS method. The bonding surface of graphite was grooved (0.2 mm wide, 0.1 mm deep, 0.4 mm apart) expecting anchor effect, and the bonding surface of W was not grooved considering the mass production of divertor component.

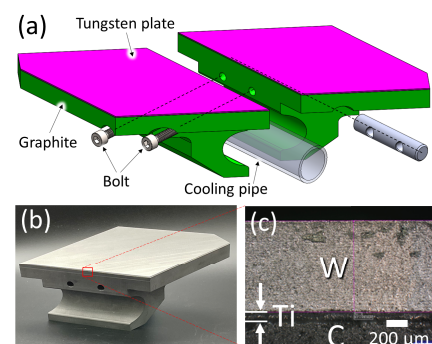


Fig. 1 (a) Structural drawing of W bonded graphite divertor component, and (b) W bonded graphite divertor block. (c) Close-up image near bonding interface.

author's e-mail: murase.takanori@nifs.ac.jp

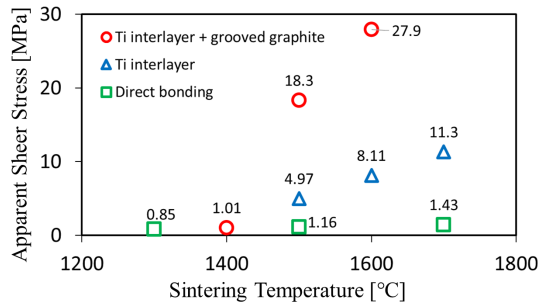


Fig. 2 Apparent shear strength of W-graphite bonding as a function of sintering temperature.

A Ti foil of 150 μm thick was used as an interlayer. The temperature, pressure and time were 1,600°C, 30 MPa, and 30 minutes, respectively, in vacuum.

To evaluate the bonding quality between W and graphite in this study, small bonding specimens (φ10 × 10 mm, each) were fabricated, and the results are shown in Figs. 2 - 4. Specimens were fabricated under several conditions with and without intermediate material and groove processing. The apparent shear strength of the small bonding specimens was measured at room temperature using an electronic universal testing machine CATY-2002S manufactured by Yonekura MFG. Co., Ltd, with a crosshead speed of 1 mm/min. In the shear test, the W section was fixed with a jig and load was applied to the graphite section from above. In addition, the bonding interface was observed using a scanning electron microscope (SEM) (JEOL JSM-6390A).

Figure 2 shows the apparent shear strength of the bonded specimens. The specimen with the Ti intermediate layer had better apparent shear strength than the direct bonded specimen, but the maximum apparent shear strength was 11.3 MPa. On the other hand, the bonded specimens with Ti interlayer and grooves showed apparent shear strength of 27.9 MPa. Groove structure increased apparent shear strength in both temperature ranges.

To investigate the effect of groove structure on the bonding strength of specimens, the fracture surface of the specimen was diagnosed by SEM. Figure 3 (a) shows the groove pattern image. As shown in Fig. 3 (c), granular structures of several μm can be observed in a groove area. The granular structure suggests the possibility of TiC formation in the grooved area as reported in a previous study [7]. However, the identification of the grain structure requires measurement by X-ray diffraction in future work. Moreover, in the non-grooved area, no granular structure is observed. In addition, the interlayer of the specimen was observed by SEM, as shown in Fig. 4. In the grooved area, we can confirm the presence of grain structure in the Ti interlayer in Fig. 4 (a). Furthermore, W, C, and Ti mapping images show that the granular structure is composed of Ti and C. On the other hand, in the non-grooved area, the diffusion of W and C in the Ti interlayer can be seen as shown

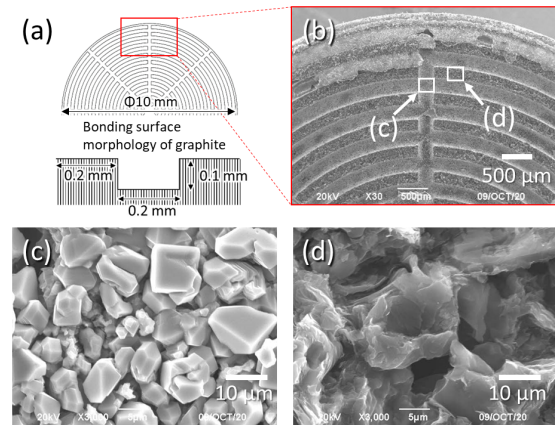


Fig. 3 The fracture surface of a bonding specimen with groove on graphite. (a) Groove pattern, (b) SEM image of the fracture surface, (c) SEM image of grooved area, and (d) SEM image of non-grooved area. There is granular structure in the grooved area.

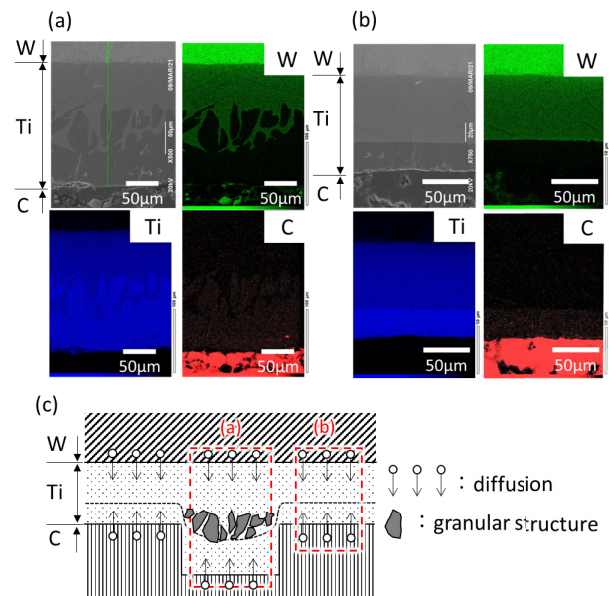


Fig. 4 SEM images and composition mapping images in (a) the grooved area, and (b) non-grooved area, (c) Schematic view of the bonding interlayer.

in Fig. 4 (b). However, no granular structure is observed.

It is assumed that the granular structure in the grooved area influences bonding strength. The effect of current and applied pressure in the SPS bonding can be linked to the development generation of the grain structure. Because of the difference in electrical resistance between Ti (0.55 μΩm) and graphite (9.2 μΩm), more current flows in the grooved area. Figure 4 also illustrates that the Ti area is thinner without the groove than it is with the groove. Because a uniform Ti foil was utilized, the portion without the groove received more pressure. The mechanism of grain structure development requires additional research in future studies.

- 
- [1] T. Yamashita *et al.*, J. Nucl. Mater. **162-164**, 841 (1989).  
[2] F. Brossa *et al.*, J. Nucl. Mater. **191-194**, 469 (1992).  
[3] X. Liu *et al.*, Fusion Eng. Des. **70**, 341 (2004).  
[4] B. Dong *et al.*, Coatings **10**, 926 (2020).  
[5] M. Tokitani *et al.*, Nucl. Mater. Energy **18**, 23 (2019).  
[6] L. Quanbin *et al.*, Weld. World **64**, 1877 (2020).  
[7] Y. Wei *et al.*, Int. J. Refract. Hard. Met. **92**, 105287 (2020).  
[8] C. Han *et al.*, Int. J. Refract. Hard. Met. **100**, 105622 (2021).